Design and Fabrication of a 3D Printed Metallic Flexible Joint for Snake-Like Surgical Robot

Yang Hu*, Lin Zhang*, Wei Li and Guang-Zhong Yang, *Fellow, IEEE*

***Abstract*—Snake-like robots have numerous applications in minimally invasive surgery (MIS). One important research topic of snake-like robots is the flexible joint mechanism and its actuation. This paper describes the design and fabrication of a new type of flexible joint mechanism which is enabled by metal powder bed additive manufacturing technique. Kinematics and static models of the flexible joint are presented, which can help in designing and controlling the flexible joint. As a compliant mechanism, the fatigue characteristics of the flexible joint is investigated. Finite Element Analysis (FEA) is also performed aiming for optimising the design process. In the experiment section, model estimation, FEA and experiment validation are conducted for further understanding the characteristics of the flexible joint. An example design that can survive after 100,000 full loading cycles is demonstrated. Finally, different design variations of the proposed method and a multi-section flexible endoscope using the proposed design are introduced. The proposed flexible joint has the potential not only in reducing the cost of manufacturing and assembling a snake-like surgical robot, but also benefits for developing of more sophisticated 3D snake robotic structure which has an optimised space for embedded sensing and actuation.**

I. Introduction

Minimally invasive surgery was introduced to ameliorate intra-operative trauma and postoperative scar, leading to reduced wound healing time, associated pain and risk of infection. The key technical requirement for MIS is the ability to adequately observe and operate a target anatomy from access sites that are not aligned in the most direct and ergonomically optimum positions. To provide surgeons with adequate visual feedback and enable dexterous tissue manipulation, endoscopes and other operative surgical instruments are necessary to have a section that is bendable and steerable. This section can be a short wrist for deflecting a surgical instrument, or a longer section, such as a continuum snake-like robot for passing through the surgical anatomy. Pulling tendons are commonly used to drive these structures. In this paper, we call the tendon driven flexible and steerable section as a flexible joint.

The first category of flexible joints achieves bending behaviour by connecting a series of small mechanical joints and routing tendon through all the joints. Almost all the typical mechanical joints can be seen in designs of the flexible joints for surgical applications. For example, the serially connected revolute joints are used in the da Vinci® 5mm tools [1] and the FlexDex surgical tools [2]. The stacking of rolling contact joints is used by Samsung® Electronics for building a variable stiffness endoscopic robot [3]. The double layer nested continuum robot with spherical joints was adopted to build a snake-like robot with lead-following ability [4] and workspace augmentation [5]. The above designs, nonetheless, are assembled piece by piece after all the parts are manufactured. A monolithically manufactured flexible joint can alleviate the manufacturing and assembling effort. For example, a flexible joint can be made by using a laser tube cutting technique to create a chain of interconnected hinge-like joints [6, 7].

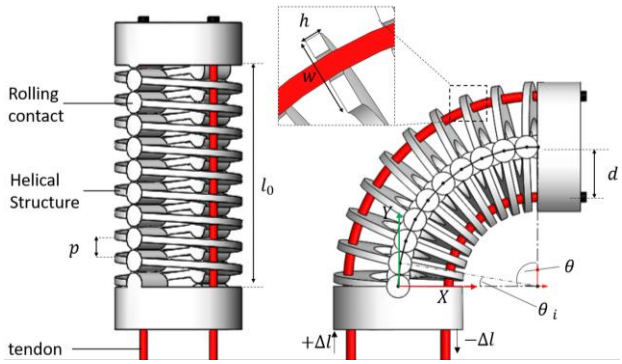

Figure 1. The CAD of the proposed flexible joint with 1-DoF bending and nomenclature used in this paper

The second category of flexible joints achieves bending behaviour by relying on the material's elastic property. The continuum mechanisms with super-elastic NiTi backbone and push-pull actuators [8] fit into this category. To create a thin flexible joint with a large central lumen, it is common to create flexure features on the surface of a NiTi tube by using laser cutting, wired EDM or CNC manufacturing techniques [9-12]. In addition to these reductive manufacturing techniques, additive manufacturing techniques, such as selective laser sintering, are also used to monolithically produce the continuum robot based on flexure structures [13]. The use of off-the-shelf helical springs [14, 15] to build flexible joints is also common. These designs have the advantage that the stress is more uniformly distributed [16] than the flexure-based designs, thus causing less fatigue issue.

A more comprehensive description on the designs of the flexible joint is provided by Jelínek et al. [17]. The first category

* These authors are equally contributed to the paper.

This project is funded by EPSRC (EP/L020688 and EP/P012779/1) and the Wellcome Trust Institution Translation Partnership Award and patented (GB 1812622.7). Yang Hu, Lin Zhang, Wei Li and Guang-Zhong Yang are with the Hamlyn Centre for Robotic Surgery, Imperial College London. {y.hu12, lin.zhang, wei.li16, g.z.yang}@imperial.ac.uk

TABLE I. NOMENCLATURE USE IN THIS PAPER

Sym.	Description
d	Moment arm of the pulling tendon [mm].
F	Tendon pulling force [N]
M	Bending moment [N·mm]
θ	Angular deflection of the flexible joint [rad]
n	Coil Number
l_0	Rest length of the flexible joint [mm]
Δl	Tendon pulling length [mm]
r_{mc}	Mean coil radius [mm]
I	Second moment of area [mm^4]
J	Polar second moment of area [mm^4]
E	Young's modulus [MPa, $\mathrm{N/mm}^2$]
G	Shear Modulus [MPa, $\mathrm{N/mm}^2$]
p	Pitch of the helical structure [mm]
h	Height of the cross section of the rectangular spring wire [mm]
w	Width of the cross section of the rectangular spring wire [mm]
γ	Compensation factor for rectangular cross section spring wire.
$\emptyset_{od}$	Outer diameter of the flexible joint [mm]
$\emptyset_{od}$	Inner diameter of the flexible joint [mm]

is based on using a series of small mechanical joints. Friction, either significantly high or negligibly small is the dominant force which dictates the bending shape [17]. Due to the nonlinear property of friction, the bending angle of each small joint may not be equal, resulting in a non-uniform bending curvature. The second category utilising material elasticity can have a smoother body shape. However, the beam flexure structure can easily cause stress concentration in the corners; fatigue and fracture may occur after thousands of loading cycles [9]. The helical spring structure has longitudinal compression and extension, which is an undesirable behaviour for a flexible joint. Some flexible joint designs combine features of the two categories. For example, Suh et al. [18] proposed a continuum robot design with the rolling contact joints linked by NiTi backbones. Kato et. al [19] created a two layers continuum robot, which has the rolling joints outside and a notched NiTi tube backbone inside.

In this paper, we would like to demonstrate a patented, monolithically produced flexible joint (Patent Number: GB 1812622.7). The flexible joint takes advantage of the rolling contact joints and the compliant structure. The proposed flexible joint is designed with the aid of FEA and manufactured by utilising a 3D metal printing, called laser melting (SLM) technique. With a special consideration on the design and manufacturing process, ready-to-use flexible joints for surgical instruments are produced. The design can survive 100,000 full loading cycles without breaking.

The remainder of the paper is organized as follows. Section II briefly introduces the design and manufacturing process of the flexible joint. The kinematics and static modelling are performed. Fatigue analysis will be discussed and the FEA method will be explained. Section III demonstrates a comparison study with theoretical estimation, FEA and the experimental test. Based on the theory presented in Section II, an FEA aided optimal flexible joint are designed and tested. In Section IV, variations of the proposed flexible joint are proposed, and a multi-section design of a flexible endoscope is presented as an exemplar of robotic applications. Section V povides an discussion of the proposed flexible joint in terms of cost and manufacturing techniques. Section VI provides the conclusion and future consideration of the work.

II. DESIGN AND FABRICATION

A. Design Overview

The CAD model of the proposed flexible joint is shown in Fig. 1. The nomenclature used in the paper is listed in TABLE I. The design is based on a helical spring-like structure, which serves as the bending backbone. Antagonised pulling tendons are routed through the guiding channels inside the helical structure and terminated at the structure's distal end. To prevent the undesirable axial compression of the helical structure, a series of circular rolling contacts are introduced at each turn of the helix. The diameter of the rolling contact equals to the pitch of the spring. The rolling contacts are arranged along the helix and radially spaced apart from each other by 180°. Driven by two tendons, each structure can perform 1-DoF planar bending. In addition to preventing axial compression, the circular rolling contacts also serve as constraints which only allow relative movement along their circumferences. The proposed design has the following advantages compared with other types of flexible joint.

- It has a large central lumen for passing the tendons or electronic wires for the distal functional part.
- It has less stress concentration and longer fatigue life, because stress can be more uniformly distributed for bending a helical structure. The channels for routing the tendons can be easily created by using the 3D printing technique.
- It is a monolithic compliant structure, which requires less manufacturing and assembling effort.
- The compliant property of the new design makes sure that the flexible joint has a smooth bending curvature and the constant bending curvature assumption can be applied in the control modelling procedure.

B. Kinematics and Static Modelling

By pulling the tendon terminated at the distal end of the flexible joint with force F, the tension is transduced into a bending moment $M = dF$, which will bend a single helical turn structure with a small angle θ_i. By ignoring the friction between the tendon and the small guiding channel, the bending moment applied to each spring turn is equal. If the coil number for the spring-like structure is n, the total bending angle is as Eq. (1)

$$\theta = n\theta_i \quad (1)$$

Under the assumption of constant bending curvature, the relation between tendon pulling length and the bending angle of the flexible joint can be calculated by Eq. (2):

$$\Delta l = d\theta \quad (2)$$

To model the relationship between tendon pulling force and the bending angle, we need to introduce several simplifications and assumptions. Firstly, as the flexible joint is based on helical spring, the rolling contacts may have a very small contribution to the flexural rigidity of the bending structure. We can therefore consider bending of the flexible joint as bending of a rectangular wire helical spring under a pure moment applied at its distal end. We select a rectangular wire cross-section, because it is easier to print than circular cross-section. Secondly, the friction between the tendon and its guiding channel is very small which can be ignored. Previous research has performed extensive research on mechanical springs [20]. We follow the same theory to derive the statics of a lateral bending helical structure.

When a spring undergoes bending, the wire of the spring is subjected to both torsion and flexure. For a single coil spring i, the angular deflection θ_i can be calculated as:

$$\theta_i = \gamma \pi M r_{mc} \left(\frac{1}{EI} + \frac{1}{GJ}\right) \quad (3)$$

$$r_{mc} = \frac{\emptyset_{od} + \emptyset_{id}}{2} \quad (4)$$

$$I = \frac{wh^3}{12} \quad (5)$$

$$J = \frac{wh(w^2 + h^2)}{12} \quad (6)$$

where r_{mc} is the mean coil radius, I is the second moment of area for the rectangular section of the spring wire, w is the width of the rectangular section and h is the height, J is the polar second moment of area for the rectangular section, $M = dF$ is the moment applied at the distal end of the single coil spring. Inspired by [20], in which a compensation factor γ is introduced for modelling the relation between the axially loading force and the spring compression for a rectangular wire spring, here we also use a compensation factor γ for the lateral bending case.

If the helical structure's coil number is n, then the relation between the tendon pulling force and the total angular deflection θ can be calculated as:

$$\theta = n\gamma \pi F d r_{mc} \left(\frac{1}{EI} + \frac{1}{GJ}\right) \quad (7)$$

As described by Eq. (7), we can firstly refer that θ and F are linearly dependent when working within the material's elastic range, which obeys Hooke's law at the state of equilibrium. Secondly, pitch p has no influence in Eq. (7), which means, ideally, for springs with different lengths, if the coil number and wire geometry is same, then θ and F follows the same relation. However, a smaller pitch can make the structure more compact; a larger pitch can increase the maximum bending angle of the structure. Thirdly, both w and h influence the bending stiffness, which is defined as the force divided by the bending angle.

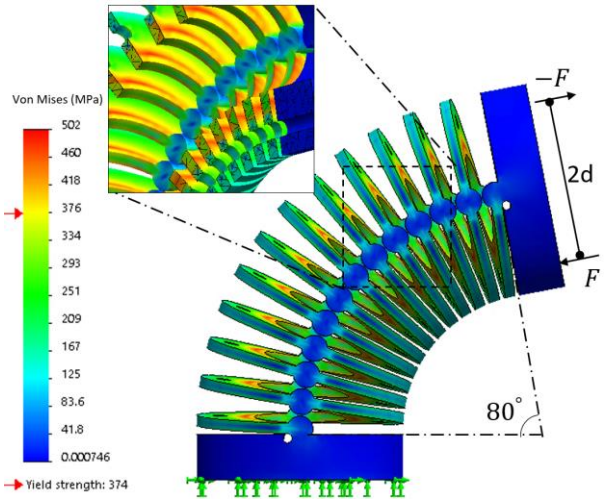

Figure 2. The FEA of an optimally designed flexible joint which has 12 helical turns. A bending moment (a force couple) is applied on the distal end, which causes a bending angle of $\theta = 80^{\circ}$ and the maximum von Mises

C. Manufacturing

The flexible joint is manufactured by a metal powder bed additive manufacturing technique, called selective laser melting (SLM). It is a 3D printing technique, which prints layer by layer of metal powder, using the laser to fuse the material in each layer and eventually forms a solid 3D part. The design demonstrated in this paper is produced by the Concept Laser Mlab and the material adopted is stainless steel (CL20ES). To print a 3D part with structure hanging in the air (or hollow structure), a support structure needs to be created for supporting the hanging surface. This support structure has a lower density which is easily removed after printing. Due to the principle of the SLM technique, the structure can incline less than 45° angle with the horizontal plane without adding support material. During the printing setup, orientation for placing the helical structure is very important. In additive manufacturing, features which are very closed to each other will fuse together. To prevent the fusion of two neighbouring rolling circular contacts, their minimal distance is set with 0.035mm. When printing a circular channel horizontally, if the channel diameter is large, support structures are required to support the ceiling of the channel. Without support structures, the part may deform. However, in our case ($\emptyset_{od}$ =9mm, $\emptyset_{id}$ =4mm), this deformation is very small, less than 4%, so we did not add support structure inside the channel. If high accuracy is required, the support structure can be added and later be removed by wire EDM technique.

D. Fatigue

Fatigue is a general concern when using SLM technique for manufacturing compliant metallic parts. The little cracks of the metal printed part and the unpolished surface is supposed to cause fatigue for cyclic loading applications. As reported by Todd M. Mower et.al. [21], the 316L stainless steel parts produced by the

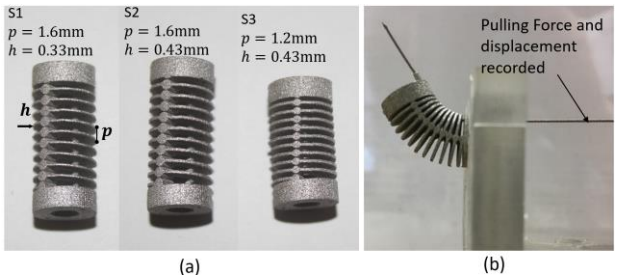

Figure 3. (a) Three flexible joint specimens S1, S2 and S3 have been manufactured to validate the FEA results. Their outside and insider diameters are $\emptyset_{od}$ =9mm, $\emptyset_{id}$ =4mm. (b) To test the relationship between the tendon pulling force and the bending angle, one tendon is used to pull the flexible joint to bend. The tendon pulling length is measured with a caliper and the tendon pulling force is measured with force gauge. The bending angle can be calculated from tendon pulling length using Eq. (2).

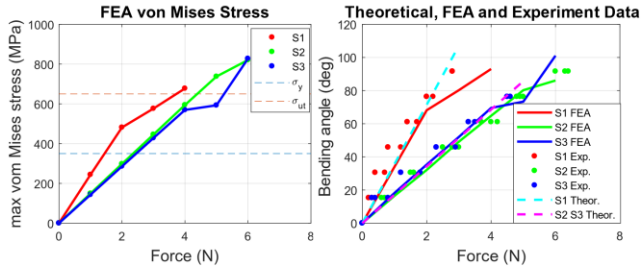

Figure 4. (Left) The relationship between the force couple and the maximum von Mises stress for each specimen as obtained from FEA result. The test is performed by increasing the force with step size 1N and record the bending angle. The solid lines are the interpolation of the discreet testing points. (Right) The thermotical estimation, the FEA results are shown together with the experiment result. For the theoretical estimation, γ is empirically selected as 2.5.

SLM technique may have even higher yield strength, but the same elastic modulus compared to the machined parts. However, the SLM parts may be more prone to fatigue under cyclic loading. In the fatigue test, stainless steel parts fabricated in the horizontal orientation presented almost equal average lifetime to those made by wrought material but are with greater variation. The fatigue strength of vertical build parts at lifetimes $10^5 - 10^6$ cycles has only 30% of the horizontally printed parts. Similar results were demonstrated by Spierings et. al. [22], who performed fatigue tests with the 316L stainless steel parts produced by a Concept Laser Mlab machine. According to their test, the endurance limit of the 316L specimens is around 280 MPa and the tensile strength is around 650 MPa. When the max stress in a sample is around 500 MPa, the number of cycles to fail is around 100,000. We will design the proposed flexible joint following the guidance of the S-N curve in [22]. In addition, as reported by [21], post-processed with hot isostatic pressure (HIP) process can also improve the high-cycle fatigue behaviour. The vertically-built specimens with HIP can generate high-cycle fatigue strengths of approximately 50% (without HIP is 30%) of that of the horizontally-built specimens without HIP. As suggested by the manufacturer of the Concept Laser machine, the printed 316 parts are recommended to be heated up in 3 hours to 550°C. Maintain temperature for 6 hours. Subsequently allow the component cooling down in the oven or at ambient temperature.

E. Finite Element Analysis

Despite extensive analytical work on helical spring, such as Whal et al [20], previous analyses are mostly based on regular shaped spring wires instead of irregular cross section wires, such as the proposed rolling contact aided structure, making Eq. (7) inaccurate for describing the flexible joint. To achieve a design with optimal performance, detailed FEA is required for stress and deflection computation. The theoretical model can be used for an initial estimation and final verification.

In this work, FEA is performed by the nonlinear static simulation provided by SolidWorks Simulation Premium, which can be used for different analysis such as static, frequency, buckling, thermal and topology optimization. Fig. 2 illustrates the FEA result of a bending flexible joint. SolidWorks Simulation cannot direct ly apply a moment to a solid model. In this simulation, a force couple ($-F, +F$ and arm $2d$) is used to simulate a moment. The forces are applied normally to the position where the tendons terminated. Most importantly, the force couple should be updated to be always perpendicular to the face when the face is deflected. This function should be selected before starting SolidWorks nonlinear static simulation. As shown by Fig. 2, when a bending moment applied to the distal end of the flexible joint, it bends to a constant curvature shape with the neutral axis located in the centre of the structure. The stress distribution is similar with the result presented in [16]. The maximal von Mises stress appears in the inner side of the spring wire, which is explained in both references [16, 20]. The stress near the neutral axis is small, even though it has a larger discontinuity due to the circular contact. Under a pure distal moment, the length of the flexible does not change, which can be verified by that the two neighbouring circular rolling joints did not penetrate each other during the bending simulation.

III. EXPERIMENT

In this section, a cross validation of the theoretical estimation, FEA results and experiments on real samples is presented. By comparing the data obtained from different sources, we can test the correctness and reliability of each method. We will subsequently use the knowledge obtained in the experiment for optimally designing a flexible joint which could meet the special geometrical and fatigue life requirements.

A. Validation of the Modelling and the FEA with Experiment

Three prototypes, S1, S2 and S3, as Fig. 3 (Left), were used to validate the reliability of the modleing and the FEA. In this experiment, the tendon pulling force and the bending angle of the flexible joint were recorded as illustrated by Fig. 3 (right). The two design parameters to be investigated are the height h of the rectangular wire's cross section and the pitch p of spring. S1 and S2 have different h and same p. S2 and S3 are with different p

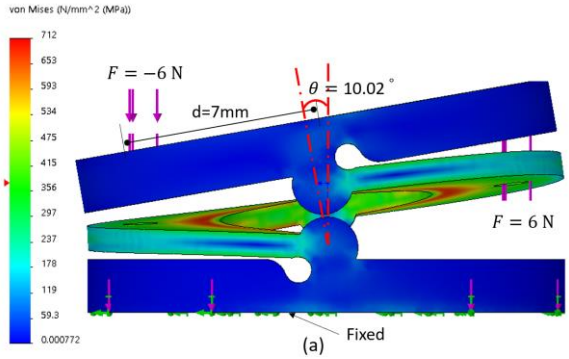

Figure 5. (a) The FEA result for a single helix segment with a moment (a force couple) applied on its tip. The structure bends to an angle θ and the maximum von Mises stress is 712 MPa. (b) The relationship between the bending angle and the max von Mises Stress for a single helix design ($p = 1.2mm, h = 0.45mm, \emptyset_{od}$ =9mm, $\emptyset_{id}$ =4mm).

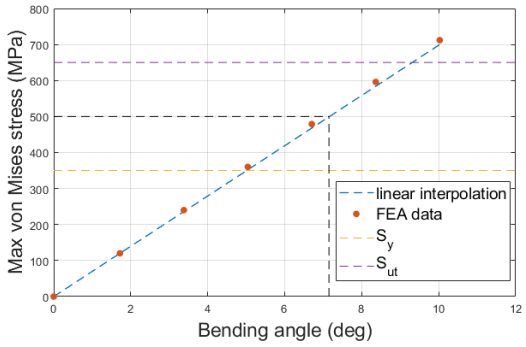

Figure 6. The relation between the bending angle and the max von Mises Stress for a single helix design ($p = 1.2mm, h = 0.45mm, \emptyset_{od}$ =9mm, $\emptyset_{id}$ =4mm).

and same h. For each specimen, three identical tests were performed, and the results presents the average of the three tests. During the test, we found that there is a hysteresis phenomenon for the data measured during the bending and unbending phase. The hysteresis (0.2N-0.5N different between bending phase and unbending phase) presented in all tests. The hysteresis could be caused by the friction between the tendon and its guiding channel. Plastic defamation could also cause hysteresis, but it is unlikely in this case, because the samples which can survive 100,000 loading cycles also present hysteresis in the bending/unbending test.

In order to keep the consistency when comparing with the FEA results, we only use the data measured during the bending phase. FEA was performed for each specimen with the method mentioned above. Fig. 4 (Left) shows the relation between the magnitude of the force couple and maximal von Mises stress obtained by the FEA. The relation is linear when the maximal von Mises stress is low and later become nonlinear as the stress increases. Fig. 4 (Right) plots three data sets obtained from the theoretical estimation, the FEA and the experiment respectively. The experiment data is shown at measuring points. For each sample, the bending experiment was performed 3 times, so there are 3 sets of measurement data for each sample. The FEA results are interpolated as solid lines. The dash lines show the estimation using Eq. (7). As illustrated, the three data sets roughly conform with each other even though some disparities exist. The corresponding data for S1 tends to have a larger disparity than S2 and S3. This disparity may be caused during the manufacturing and post processing procedure. The structure of S1 ($h = 0.33$) is weaker than S2 ($h = 0.43$) and S3 ($h = 0.43$). More deformation may be caused when S1 is mechanically removed from the printing tray. Another disparity appears when the maximal von Mises stress exceeds 560MPa. As the loading force increases, the caused deformation exceeds the material's elastic range. The FEA results appear nonlinear, but the experimental results remian linear even though permanent deformation is caused. As the maximal von Mises stress exceeds 560MPa, the FEA is no longer accurate. As evident from both the experimental data and the FEA data, S2 has slightly higher bending stiffness than S3. Without the circular rolling contact, they should have the same bending stiffness. However, as the pitch increases, the circular rolling contact becomes larger, which makes S2 stiffer than S3. By empirically selecting the compensation factor γ as 2.5, the estimation for all the specimens can roughly fit with the experiment and FEA data. The Young's module and shear module for the selected 316L material are 200,000 MPa and 34, 200 MPa. As pointed by [20], the compensation factor has a small variation with the ratio of w/h. From the above results, it can be concluded that the FEA performed by SolidWorks nonlinear static study can be used when the maximal von Mises stress is less than 550MPa. The FEA can be adopted as a useful tool for designing the flexible joint with prescribed fatigue life. The static estimation with Eq. (7) can be used as a rough calculation at the design beginning stage; however, the compensation factor should be known first, which can be estimated beforehand as a look-up table based on the FEA results.

B. FEA Aided Optimal Design

When designing the flexible joint for optimal performance, there are some parameters that need to be tuned. Even though FEA can be applied to every design achieved by trial-and-error, it can be time-consuming. To speed up the design process and obtain an optimal performance, a method was proposed as follows.

In an example, the proposed design is used for the flexible neck of a steerable endoscope. The flexible neck is required to have a 1 DoF bending which can position the camera head on its tip in various viewing angles. The length of the flexible neck is required to be as short as possible to work in a confined space. Its outer diameter is preselected as $\emptyset_{od}$ =9mm and a central channel is $\emptyset_{id}$ =4mm for routing the electronic and optical cables for the camera head. The maximum bending angle should be larger than 80°. As $\emptyset_{od}$ and $\emptyset_{id}$ are preselected, the width of the rectangular wire is 2.5mm. The height of the rectangular wire should be larger than 0.45mm to achieve a strong structure. For the circular rolling contact, to make it printable with the Concept Laser SLM technique, it should be larger than 1.2mm. Finally, the life of the

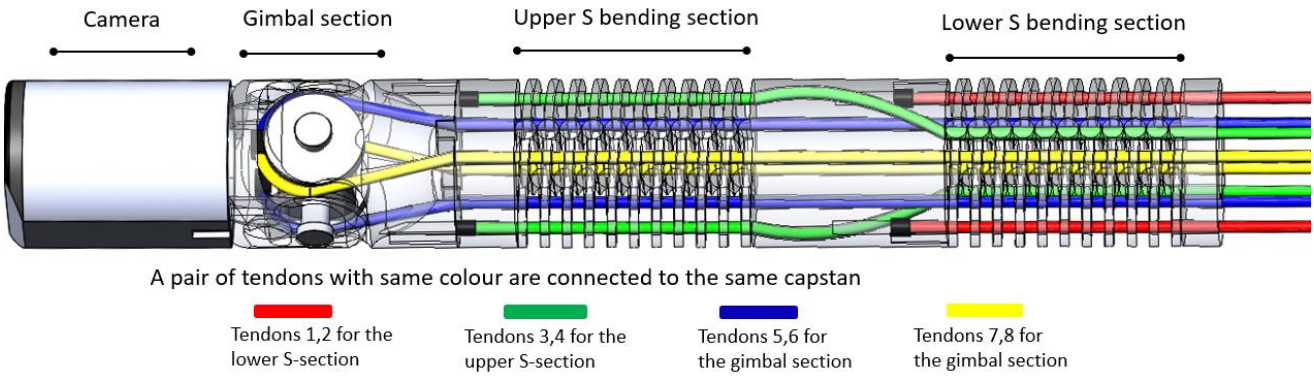

Figure 7. Tendon layout of an S-bending flexible endoscope designed for an single-port surgical system. The device has two flexible sections, which can form into an S-bending shape. The gimbal located at the distal end provides an independently contolled tilt and pan movment for the camera head.

flexible neck is supposed to be around 100,000 bending cycles, so the maximal von Mises stress should be below 500MPa as shown by the S-N curve, as indicated by [22]. The above description can be formulated as follows:

$$\text{Minimize } (l_0) \tag{8}$$

subject to

$$l_0 = np \tag{9}$$

$$\theta_{max} \geq 80° \tag{10}$$

$$l_0 - \theta_{max} d > nh \tag{11}$$

$$\sigma(\theta = 80^{\circ}) < 500\text{MPa} \tag{12}$$

$$p \geq 1.2\text{mm} \tag{13}$$

$$h \geq 0.45\text{mm} \tag{14}$$

For Eq. (9), it describes that the rest length of the bending neck equals to its coil number multiplied by its pitch. Eq. (11) means when the flexible neck bends to 80°, the two neighbouring coils should not contact with each other. Combining Eq. (9-11), it can be inferred that the coil number n should be larger than 7.33.

Beside geometrical constraints, another factor that affects selection of the coil number is described as Eq. 12, when the flexible bends to 80°, its von Mises stress should not exceed 500MPa . To determine the minimal coil number, FEA is performed for a single turn helix structure with $p = 1.2\text{mm}$ and $h = 0.45\text{mm}$. One end of the structure is fixed, and a force couple is applied to the other end of the structure. The bending angle and max von Mises stress is recorded. Fig. 5 shows the FEA test performed with the single helix structure. When the bending angle is $\theta = 10.02°$, the maximal von Mises stress shown by the legend is 712 MPa. Fig. 6 plots the relation between the bending angle and the maximum von Mises stress. To ensure that the maximum von Mises stress is less than 500 MPa, the bending angle for a single turn should be smaller than 7.12°. So, to bend 80°, the coil number n should be larger than 11.1. By selecting n larger than the bigger value between 7.33 and 11.1, n=12 is used. Fig. 2 has shown the FEA results for the target design. When the flexible joint bends to 80°, its maximum von Mises stress is around 500MPa, which satisfies the requirement. Based on the design parameters ($n = 12$, $p = 1.2\text{mm}$, $h = 0.45\text{mm}$, $\emptyset_{id} = 4\text{mm}$, $\emptyset_{od} = 9\text{mm}$), the flexible joint is manufactured with the SLM technique and a fatigue test was performed. After 100,000 cyclic loading (bending to 80° by pulling the tendon and unbending to its neutral position), the flexible joint did not appear any visible fracture and the overall stiffness of the structure did not change either.

IV. Design Variations

A. Multi-Section Design

By combining multiple sections of the proposed design, a a long snake-like robot can be built for more complex surgical tasks. A flexible endoscope with the flexible joints, as shown in Fig. 7, is designed for a single-port surgical robot system. It has an S-shape body and 2-DOF gimbal tip. For a single-port surgical robot, it passes all the surgical instruments, including the flexible endoscope through a single surgical port. The camera needs to go up in the elevation direction and look down to have an optimal view of the surgical field. This new design can fulfil the requirement. The S-shape bending changes the camera's position in elevation direction and the distal gimbal section can perform independent tilt and pan movement for the camera. In this design, helical tendon routing channels (Fig. 7) in the middle of the S-section are used for removing the crosstalk between the upper S-section and the lower S-section, the tendons for the upper S-section pass through the bending neutral axis of the lower S-section and follow a helical route in the connection area (the tendon channel has 90° rotation in the wall of the structure). With the helical tendon-routing, actuation of the upper S-section does not affect the bending shape of the lower S-section.

By leveraging the strength of additive manufacturing, it is possible to create such helical tendon routing channels which is very difficult to create with reductive manufacturing technique. With this configuration, the pulling force applied for the upper S-section will not influence the shape of the bottom S-section. For

the tendons controlling the gimbal, they are all laid out close to the neutral bending axis of the S-section, so control of the gimbal section is also decoupled with the S-section. The tendon layout for the gimbal section is similar with [23]. With this type of tendon routing, the four tendons need to synchronise to control the 2-DoF of the gimbal. It has the advantage that all the tendons are constrained by the pully system and will not get slack when driving the gimbal.

B. Other Designs

Base on the same design principle, various contact aided compliant structures can be used for the flexible joint. Firstly, the rolling contact can be replaced by the hinge-like joint which has half concave and half convex part. This type of joint has a circular contact surface. It increases the torsion stiffness of the structure, but it also occupies more space than the rolling contact joint, making the pitch larger. Secondly, double helix structure be adopted, making the structure symmetrical according to the bending plane. Thirdly, the flexible joint can have a variable pitch and the diameter of the rolling contact joints is varying with pitch. The portion with the larger pitch has higher bending stiffness, and the portion with small pitch has lower bending stiffness. In this way, it can achieve a variable bending curvature, e.g., distal end bends first, which has the advantage of increasing distal dexterity while reducing space occupation. Fourthly, the rolling contact joints as well as the tendon channels can be arranged helically. This design can have larger dexterous workspace compared with conventional tendon routing method.

V. DISCUSSION

The current trend of utilization of metal printing is moving from rapid prototyping to rapid manufacturing. The cost of SLM machine is around £100,000 -£600,000 and the material cost for producing one proposed flexible joint is less than £1. With the additive manufacturing technique, the proposed flexible joint can be monolithically produced, which also minimizes effort in the manufacturing and assembling process. To produce 3d compliant parts with metal printing techniques, the engineer should understand working principle of the technique, the machine and material properties. In the beginning design phase, trail-and-error can be used for gaining these knowledges. Based on these knowledges, FEA as well as other computer aided simulation method for predicting thermal deformation during printing can be used for optimizing the design.

Currently, the only disadvantage of the SLM technique as well as other metal printing technique is that the parts produced are with inferior mechanical property (low accuracy, more prone to fatigue and course surface) than machined parts produced by CNC, laser cutting or casting. However, the additive manufacturing technique has an irreplaceable advantage in the capability for manufacturing more sophisticated 3D snake robotic structure, which can have multiple working channels, helical tendon guiding channels and an optimised space for embedded sensing and actuation. In our opinion, at current stage, the proposed design and its manufacturing method is more suitable for producing flexible joint with diameter ranging from 5mm-20mm.

VI. CONCLUSION

In this paper, we have presented the design of a new rolling contact aided flexible joint for building snake-like surgical instruments and investigated the use of the 3D metal printing technique (SLM) to monolithically manufacture such flexible joint. The simplified kinematic model based on the constant curvature assumption and the static model based on the lateral bending of helical spring are given, which can be used as an initial estimation for selecting the design parameters for a specific application. The theoretical estimation, FEA and experiment validation are cross validated for understanding the characteristics of the flexible joint. An FEA based optimal design method for designing a flexible joint with prescribed lifetime is also proposed, which produces a flexible joint which presents no damages after 100,000 full cyclitic loading. Finally, variations of the proposed design and a multi-section flexible endoscope are introduced. We believe this work is not only valuable in surgical robot field, but also has other meaningful applications where monolithically manufactured 3D metallic compliant mechanism is required.

ACKNOWLEDGEMENT

The author would like to thank Dr. Jindong Liu and Dr. Jianzhong Shang for their valuable advice in designing and manufacturing the proposed device.

REFERENCES

[1] Ikeda, M., Rosa, D., Cooper, T. and Anderson, S., Intuitive Surgical Inc, 2005. *Cardiac tissue ablation instrument with flexible wrist*. U.S. Patent Application 11/071,480.

[2] Zimmerman, Z., Awtar, S., Johnson, B., Holmes, C.K., Costa, P.F. and Rank, R.B., Flexdex Inc, 2018. *End-effector jaw closure transmission systems for remote access tools*. U.S. Patent 9,869,339

[3] Kim, Y.J., Cheng, S., Kim, S. and Iagnemma, K., 2014. A stiffness-adjustable hyperredundant manipulator using a variable neutral-line mechanism for minimally invasive surgery. *IEEE transactions on robotics*, *30*(2), pp.382-395

[4] Degani, A., Choset, H., Wolf, A. and Zenati, M.A., 2006, May. Highly articulated robotic probe for minimally invasive surgery. In *Robotics and Automation, 2006. ICRA 2006. Proceedings 2006 IEEE International Conference on* (pp. 4167-4172). IEEE.

[5] Li, Z., Chiu, P.W. and Du, R., 2016, October. Design and kinematic modeling of a concentric wire-driven mechanism targeted for minimally invasive surgery. In *Intelligent Robots and Systems (IROS), 2016 IEEE/RSJ International Conference on* (pp. 310-316). IEEE.

[6] Liu, N., Bergeles, C. and Yang, G.Z., 2016, May. Design and analysis of a wire-driven flexible manipulator for bronchoscopic interventions. In *Robotics and Automation (ICRA), 2016 IEEE International Conference on* (pp. 4058-4063). IEEE.

[7] Brunnen, R.D. and Simon, T.J., Henke Sass Wolf GmbH, 2010. *Bendable portion of an insertion tube of an endoscope and method of producing it*. U.S. Patent 7,766,821.

[8] Xu, K. and Simaan, N., 2008. An investigation of the intrinsic force sensing capabilities of continuum robots. *IEEE Transactions on Robotics*, *24*(3), pp.576-587.

[9] Swaney, P.J., York, P.A., Gilbert, H.B., Burgner-Kahrs, J. and Webster, R.J., 2017. Design, fabrication, and testing of a needle-sized wrist for surgical instruments. *Journal of medical devices*, *11*(1), p.014501.

[10] Gao, A., Murphy, R.J., Liu, H., Iordachita, I.I. and Armand, M., 2017. Mechanical model of dexterous continuum manipulators with compliant joints and tendon/external force interactions. *IEEE/ASME Transactions on Mechatronics*, *22*(1), pp.465-475.

[11] Eastwood, K.W., Francis, P., Azimian, H., Swarup, A., Looi, T., Drake, J.M. and Naguib, H.E., 2018. Design of a Contact-Aided Compliant Notched-Tube Joint for Surgical Manipulation in Confined Workspaces. *Journal of Mechanisms and Robotics*, *10*(1), p.015001.

[12] Du, Z., Yang, W. and Dong, W., 2015. Kinematics modeling and performance optimization of a kinematic-mechanics coupled continuum manipulator. *Mechatronics*, *31*, pp.196-204.

[13] Coemert, S., Traeger, M.F., Graf, E.C. and Lueth, T.C., 2017. Suitability evaluation of various manufacturing technologies for the development of surgical snake-like manipulators from metals based on flexure hinges. *Procedia CIRP*, *65*, pp.1-6.

[14] Breedveld, P., Sheltes, J.S., Blom, E.M. and Verheij, J.E., 2005. A new, easily miniaturized steerable endoscope. *IEEE engineering in medicine and biology magazine*, *24*(6), pp.40-47.

[15] Haraguchi, D., Tadano, K. and Kawashima, K., 2011, September. A prototype of pneumatically-driven forceps manipulator with force sensing capability using a simple flexible joint. In *Intelligent Robots and Systems (IROS), 2011 IEEE/RSJ International Conference on* (pp. 931-936). IEEE.

[16] Keller, S.G. and Gordon, A.P., 2011. Equivalent stress and strain distribution in helical compression springs subjected to bending. *The Journal of Strain Analysis for Engineering Design*, *46*(6), pp.405-415.

[17] Jelínek, F., Arkenbout, E.A., Henselmans, P.W., Pessers, R. and Breedveld, P., 2015. Classification of joints used in steerable instruments for minimally invasive surgery—A review of the state of the art. *Journal of Medical Devices*, *9*(1), p.010801.

[18] Suh, J.W., Kim, K.Y., Jeong, J.W. and Lee, J.J., 2015. Design considerations for a hyper-redundant pulleyless rolling joint with elastic fixtures. *IEEE/ASME Transactions on Mechatronics*, *20*(6), pp.2841-2852.

[19] Kato, T., Okumura, I., Song, S.E., Golby, A.J. and Hata, N., 2015. Tendon-driven continuum robot for endoscopic surgery: preclinical development and validation of a tension propagation model. *IEEE/ASME Transactions on Mechatronics*, *20*(5), pp.2252-2263.

[20] Wahl, A.M., 1944. *Mechanical springs*. Penton Publishing Company.

[21] Mower, T.M. and Long, M.J., 2016. Mechanical behavior of additive manufactured, powder-bed laser-fused materials. *Materials Science and Engineering: A*, *651*, pp.198-213.

[22] Spierings, A.B., Starr, T.L. and Wegener, K., 2013. Fatigue performance of additive manufactured metallic parts. *Rapid Prototyping Journal*, *19*(2), pp.88-94.

[23] Kübler, B., Seibold, U. and Hirzinger, G., 2005. Development of actuated and sensor integrated forceps for minimally invasive robotic surger. *The International Journal of Medical Robotics and Computer Assisted Surgery*, *1*(3), pp.96-107.